Chapter 3

Results and discussion

3.1 Synthesized of ZnO-TiO_2 nanocomposites, $ZnTiO_3$, Zn_2TiO_4 and $Zn_2Ti_3O_8$

Upon dissolving of $C_4K_2O_9Ti \cdot 2H_2O$ in water, the pH dropped down to 4.3. Generally, titanium ions exist in aqueous solution as hexaaqua coordination $[Ti(H_2O)_6]^{4+}$ complex When NH_4OH was slowly added to the solution, an O–H bond of $[Ti(H_2O)_6]^{4+}$ complex was broken by transforming into the hydroxide complex or the conjugate base of the $[Ti(H_2O)_6]^{4+}$ complex. The hydroxo complex withstood olation reaction, originated by releasing of one water molecule and combining with a neighboring complex. Under kinetic control of olation reaction, bridging ligands start from cis-coordination reaction to form anatase structure. For the thermodynamic control at high temperature, nuclei of olation product start from trans-coordination reaction to form rutile structure. Hydroxide ligands were bridged (denoted by μ) between two titanium atoms. During the process, ionization and condensation kept on going even at still high pH. In the end, anatase TiO_2 was obtained. [47]

$$[Ti(H_2O)_6]^{4+} \rightarrow [Ti(H_2O)_5OH]^{3+} + H^+ \quad (3.1)$$

$$[Ti(H_2O)_5OH]^{3+} + [Ti(H_2O)_6]^{4+} \rightarrow [Ti(H_2O)_5(\mu\text{–}OH)Ti(H_2O)_5]^{7+} + H_2O \quad (3.2)$$

$$[(Ti(H_2O)_5)_2(\mu\text{–}OH)]^{7+} \rightarrow [(Ti(H_2O)_5)_2(\mu\text{–}OH)]^{6+} + H^+ \quad (3.3)$$

$$[Ti(H_2O)_6]^{4+} \rightarrow TiO_2 + 4H_2O + 4H^+ \quad (3.4)$$

In this research, anatase is considered as a metastable phase due to the cis-coordination reaction under kinetic control at low temperature and short length of time. Rutile is a thermodynamic controlling phase at higher temperature and longer time. During processing, nuclei formed and grew to be crystals, originated from order of TiO_6 octahedral units: zigzag for anatase and linear for rutile. The zigzag uses only the cis-coordination for crystal growth, but the linear requires the trans-coordination to bridge

two octahedral units. The bridging structure is unstable under kinetic control process but the linear packing is the thermal stable structure due to the closest packing of TiO_6 octahedral units. The kinetic and thermodynamic models support the irreversible process of anatase. The anatase flavors to form specific titanate (Zn_2TiO_4 and $Zn_2Ti_3O_8$) because cis-transformation tends to form under cubic crystal system. The TiO_2, Zn_2TiO_4, $Zn_2Ti_3O_8$ and $ZnTiO_3$ phases consist of TiO_6 octahedrons connected through a common edge. The anatase and spinel-like structures (Zn_2TiO_4 and $Zn_2Ti_3O_8$) have common 3D frameworks. Moreover, rutile and $ZnTiO_3$ are composed of TiO_6 octahedral layers [47]. The formation of Zn_2TiO_4 and $Zn_2Ti_3O_8$ limited by the presence of anatase and $ZnTiO_3$ can form in the presence of rutile. According to the following decomposition reactions:

$$Zn_2Ti_3O_8 \rightarrow 2ZnTiO_3 + TiO_2 \text{ (rutile) when temperature} > 820\ ^oC \quad (3.5)$$

$$2ZnTiO_3 \rightarrow Zn_2TiO_4 + TiO_2 \text{ (rutile) when temperature} > 945\ ^oC \quad (3.6)$$

Additionally, the reaction temperatures were studying from 700 ^oC for applied in calcination temperature range. All of zinc titanates were observed through XRD tecniques found that only Zn_2TiO_4 that was form pure phase in this temmperature. The explanation of this occurred were related to the main reason of surface area to voulume ratio and rutile structure factors. Surface area to volume ratio of the Zn_2TiO_4 preccursor were the highest when compare to the others precursors. Furthermore, The precursor consisted of rutile were quiet innert when compared to anatase dueto rutile was form under thermodynamic control which is the most stabled structure in TiO_2. So the temperature of $ZnTiO_3$ and $Zn_2Ti_3O_8$ were increased to 750 ^oC then obtained pure phase at this temperature as shown in fig. 3.2

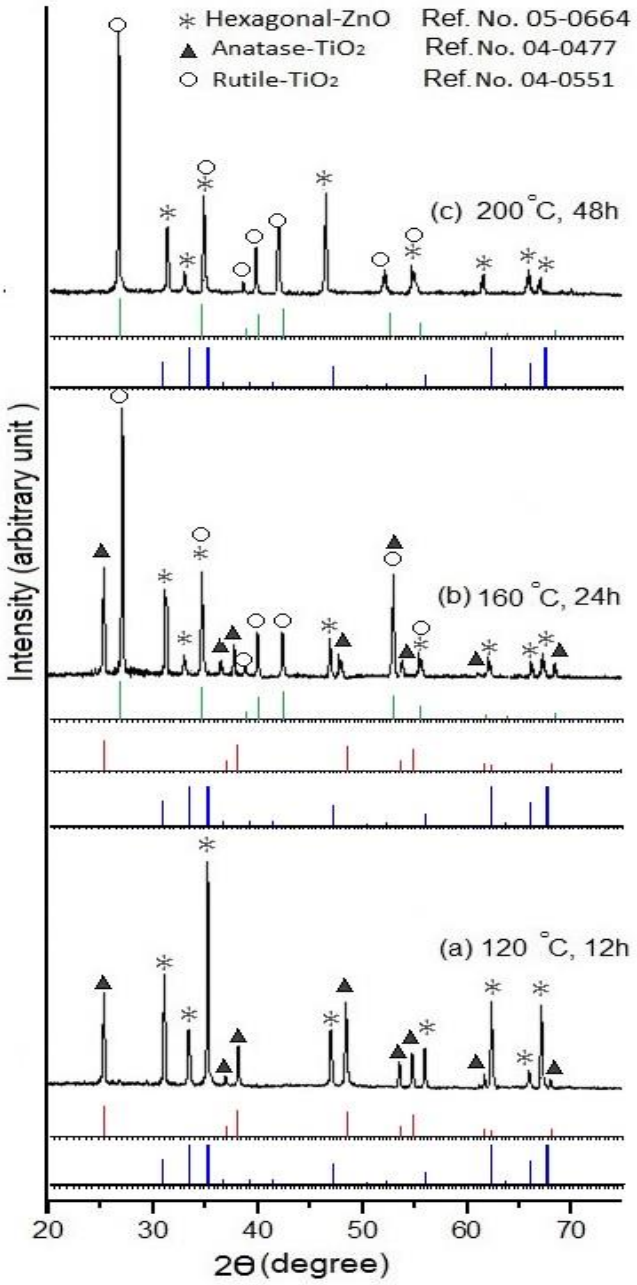

Fig. 3.1 XRD patterns of the product precursors synthesized by hydrothermal process at different temperatures and lengths of time: (a) ZnO-anatase, (b) ZnO-anatase-rutile and (c) ZnO-rutile composites.

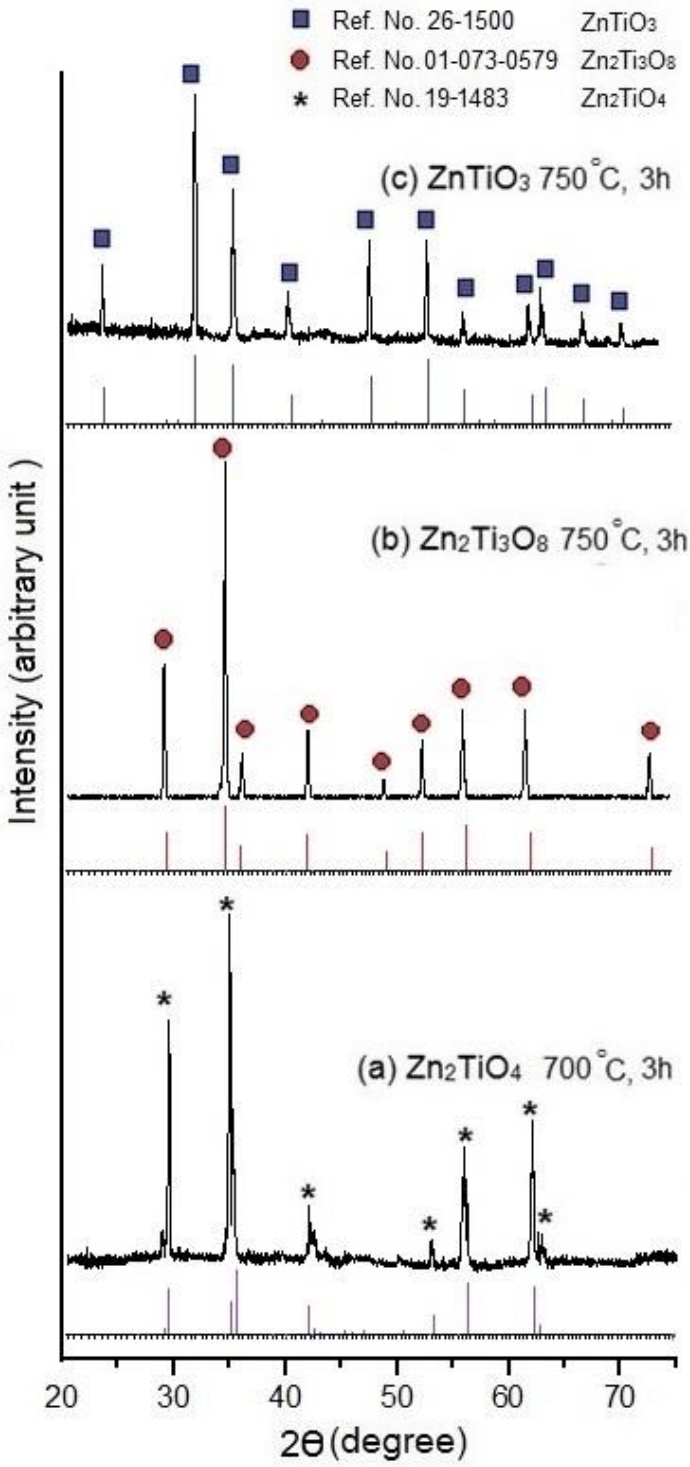

Fig. 3.2 XRD patterns of (a) Zn_2TiO_4, (b) $Zn_2Ti_3O_8$ and (c) $ZnTiO_3$.

The reactions can be avoid by using nanoprecursors and the calcination temperatures can be reduced to 700 ºC for the synthesis of Zn_2TiO_4 and to 750 ºC for the synthesis of $ZnTiO_3$ and $Zn_2Ti_3O_8$, as the XRD patterns shown in Fig. 3.2. [48]

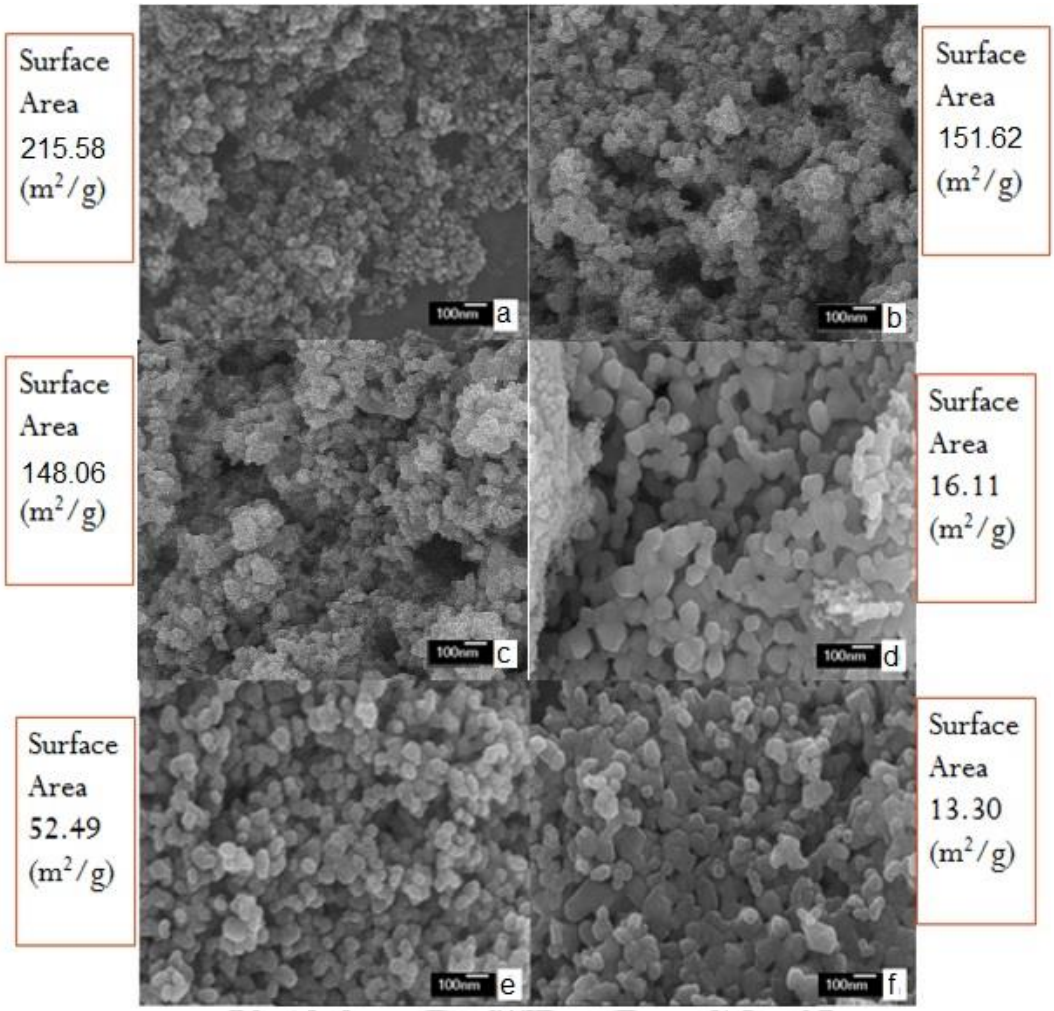

Fig. 3.3 SEM images of the (a) ZnO-anatase, (b) ZnO-anatase-rutile, (c) ZnO-rutile, (d) $ZnTiO_3$, (e) Zn_2TiO_4 and (f) $Zn_2Ti_3O_8$ samples.

Fig. 3.3 shows the morphologies and BET surface areas of ZnO-TiO_2 nanocomposites, $ZnTiO_3$, Zn_2TiO_4 and $Zn_2Ti_3O_8$. The ZnO-anatase nanocomposites synthesized at 120 ^oC for 12 h have the average diameter of <10 nm and surface area of 215.58 m^2/g that are appropriate for melting-point depression [47]. The ZnO-anatase-rutile (151.62 m^2/g) and ZnO-rutile (148.06 m^2/g) nanocomposites became larger in sequence because they were synthesized at 160 ^oC for 24 h and at 200 ^oC for 48 h, respectively. Upon calcination the ZnO-anatase nanocomposites at 700 ^oC for 3 h, the Zn_2TiO_4 nanoparticles with the surface area of 52.49 m^2/g were produced. Different atoms in the materials diffused across the boundaries of the particles. ZnO-anatase nanocomposites were chemically transformed into Zn_2TiO_4 nanoparticles with subsequent clustering together to form larger nanoparticles. During processing, counter diffusion of Zn^{2+} and

Ti^{4+} could proceed as well. $ZnTiO_3$ nanoparticles were produced by calcination of ZnO-rutile nanocomposites with 1:1 molar ratio of Zn:Ti at 750 ^oC for 3 h. Their surface area was decreased to 16.11 m^2/g. Upon calcination the Zn_2TiO_4-anatase nanocomposites at 750 ^oC for 3 h, $Zn_2Ti_3O_8$ nanoparticles with surface area of 13.30 m^2/g were produced. The main reason for increased the temperature was corresponding to surface area to volume ratio of the precursor which was the main reason to reduce the temperature influence during calcination. More surface area would provide the heat contact in the surface material and lead to increased diffusion rate of TiO_2 incorporated into ZnO structure to produce all zinc titanates faster and purer.

The trend of surface area reduction was related to temperature during calcination because of the agglomeration of the particles behavior when approached high temperature. The main reasons of agglomeration of particles was trying to reduce the heat capacity which cumulative in their surface materials. So they trying to form and diffusion to each other's under precisely stoichiometric ratio of ZnO: TiO_2 to reduce heat accumulative by fused and agglomeration then zinc titanates were obtained. The heat accumulative capacity on the materials was related to surface area of the products, higher surface area would produce fast heat accumulative. Moreover, high temperature calcination can have caused greatly reduction in surface area, too.

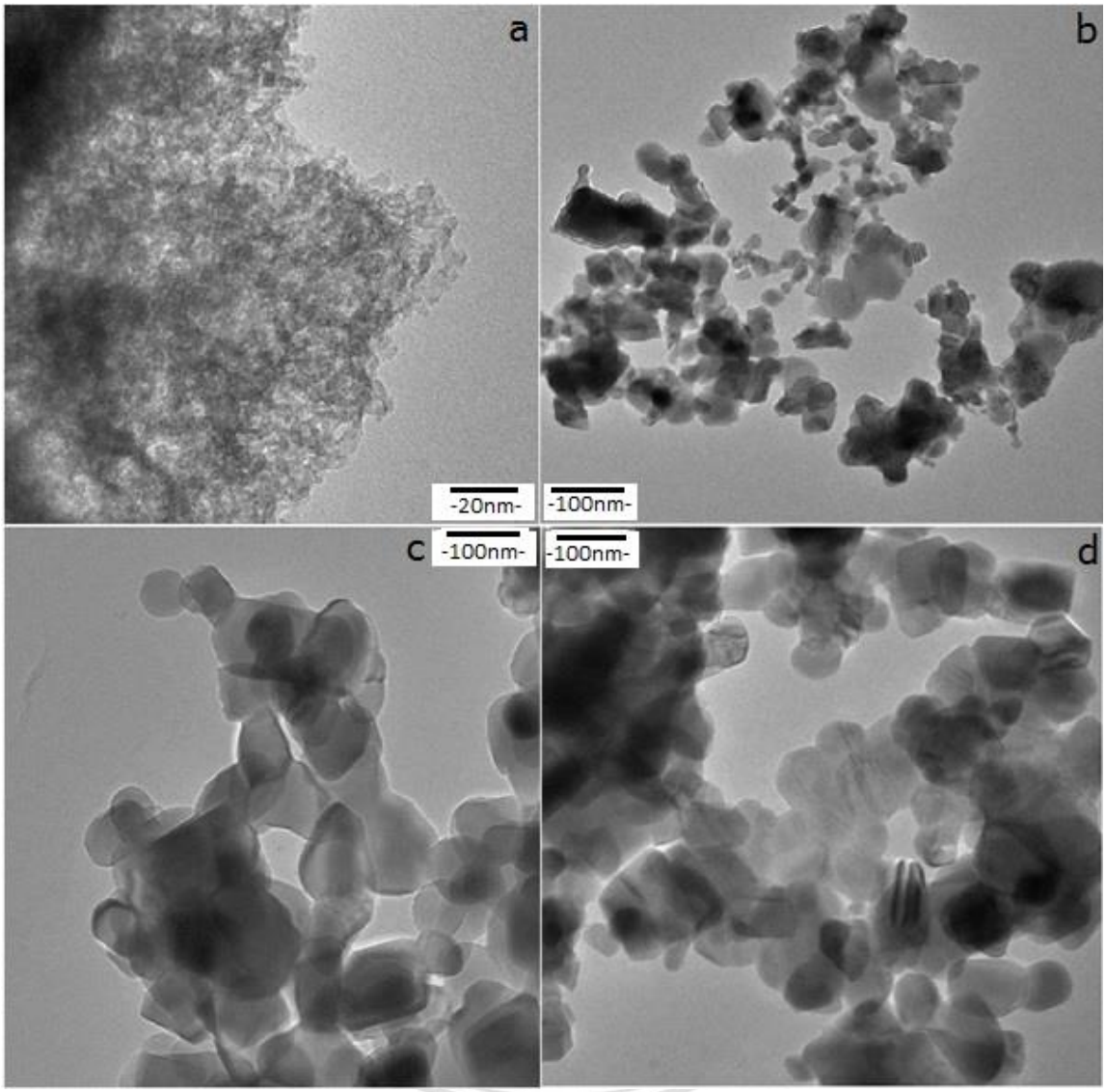

Fig. 3.4 TEM images of (a) ZnO-anatase, (b) $ZnTiO_3$, (c) Zn_2TiO_4 and (d) $Zn_2Ti_3O_8$ nanoparticles.

To further understand nanostructure and phase of the products, ZnO-anatase, $ZnTiO_3$, Zn_2TiO_4 and $Zn_2Ti_3O_8$ were characterized by TEM (Fig. 3.4) and SAED (Fig. 3.5). The TEM bright field image illustrates ZnO-anatase which was composed of very tiny nanoparticles (<10 nm diameter) and the corresponding SAED pattern of ZnO-anatase nanocomposites. In general, the melting temperature (T_m) of nanoparticles is considered to be controlled by particle size. For nanoparticles, the surface area to volume ratio is large and the surface curvature is high. The melting temperature is size dependent and is the main objective to synthesize the nanocomposites by low

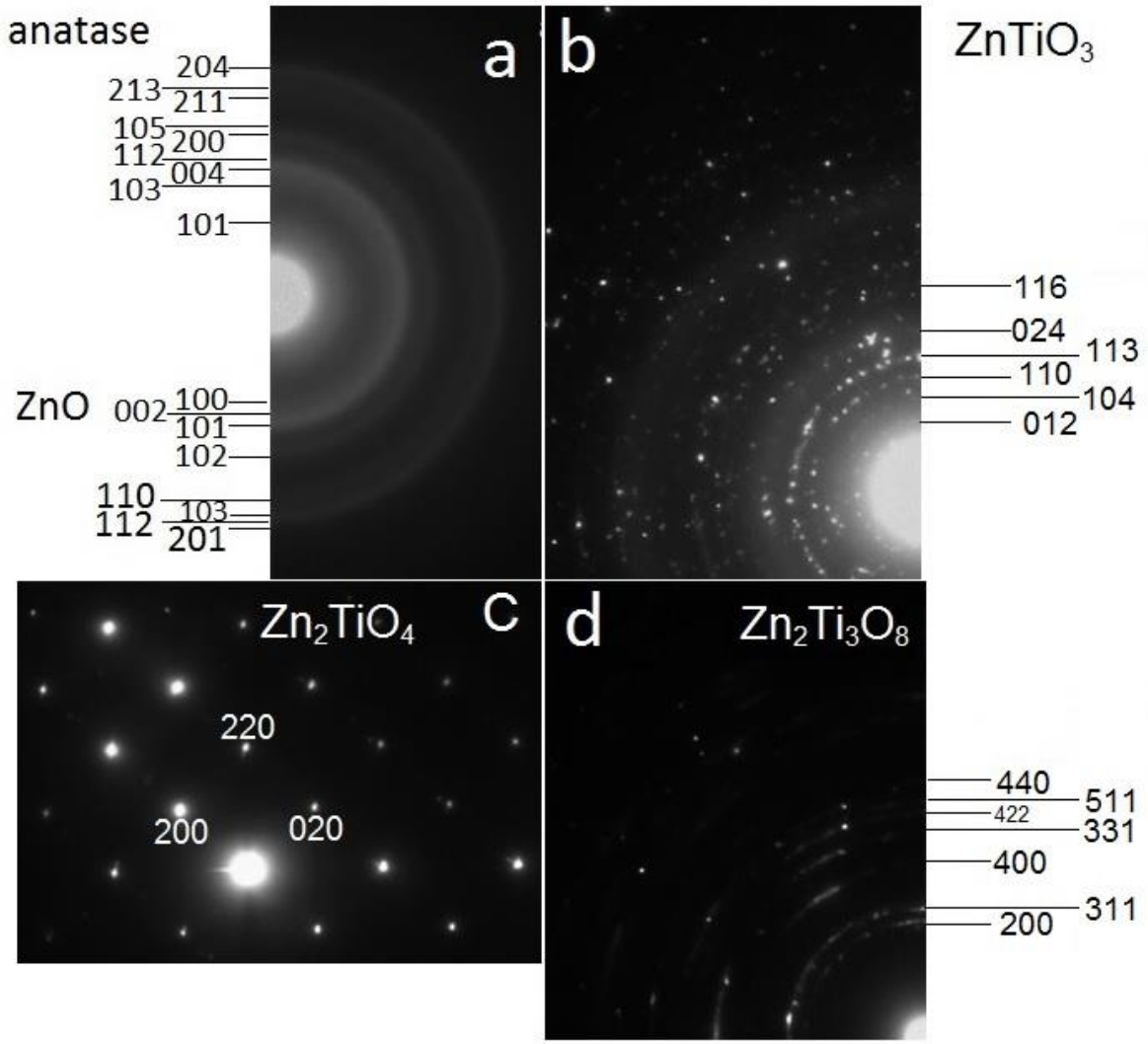

Fig. 3.5 SAED patterns of (a) ZnO-anatase, (b) $ZnTiO_3$, (c) Zn_2TiO_4 and (d) $Zn_2Ti_3O_8$ nanoparticles.

Photoluminescence (PL) of the zinc titanate samples taken with an excitation wavelength of 250 nm is shown in Fig. 3.6. Both Zn_2TiO_4 and $Zn_2Ti_3O_8$ show strong PL emission at 386 nm and a weak band at 325 nm. Weak violet emission of Zn_2TiO_4 and $Zn_2Ti_3O_8$ was detected at 280 nm. In contrast, $ZnTiO_3$ shows a strong PL peak at 370 nm only. This detection belongs to hexagonal limonite type $ZnTiO_3$ [50]. Based on SAED and TEM results, Zn_2TiO_4 is the only perfect single crystal which could perform the best PL emission. The $Zn_2Ti_3O_8$ phase caused reduction in crystalline degree, resulting in quenching of PL sensitivity. Its emission was at the middle because it contained both Zn_2TiO_4 and $2TiO_2$. In case of $ZnTiO_3$, the emission was the lowest because the transformation stable phase-rutile and ZnO were very difficult comparing to

anatase metastable-phase. The real material system always incorporates in disorder. Structural defects and lattice disorder are the cause of vibration and variation of chemical composition. Thus the system containing defects is not an interesting optical material.

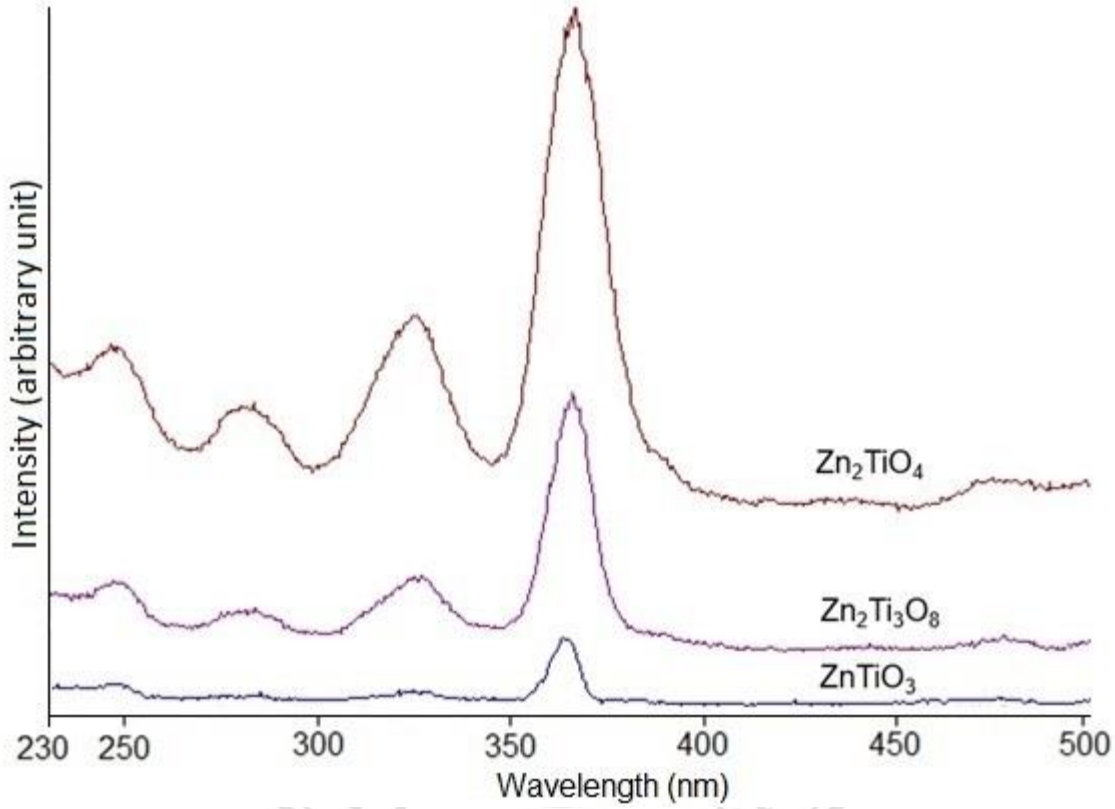

Fig. 3.6 Photoluminescence of $ZnTiO_3$, $Zn_2Ti_3O_8$ and Zn_2TiO_4.

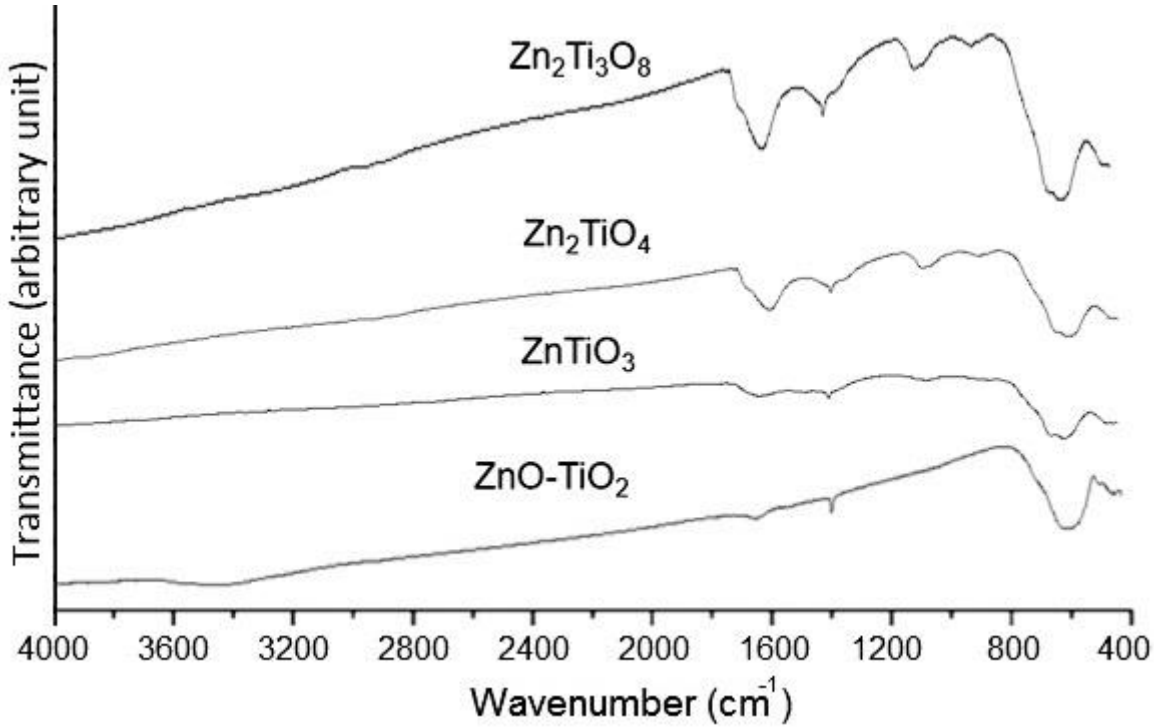

Fig. 3.7 FTIR spectra of ZnO-anatase, $ZnTiO_3$, Zn_2TiO_4 and $Zn_2Ti_3O_8$.

FTIR spectra of ZnO-anatase, $ZnTiO_3$, Zn_2TiO_4 and $Zn_2Ti_3O_8$ are shown in Fig. 3.7. Vibration of [TiO_6] and Zn–O–Ti groups existing in different phases of the products were detected at 550–650 cm^{-1} and 735 cm^{-1}, respectively. The wavenumber for Ti–O octahedral absorption of titanate increased with decrease in Zn:Ti molar ratio. The ZnO_4 stretching vibration was detected at 400–500 cm^{-1}. Some residual oxalate groups were detected at 1400–1600 cm^{-1} [49].

Raman spectra of ZnO-anatase, Zn_2TiO_4, $Zn_2Ti_3O_8$ and $ZnTiO_3$ are shown in Fig. 3.8 ZnO has a wurtzite crystal structure with $P6_3mc$ space group. Its vibration modes are generally predicted by the optical theory group $A_1 + 2E_2 + E_1 + 2B_1$ [51]. The A_1 and E_1 phonon modes are both Raman and IR active, the E_2 mode is only Raman active, and the B_1 mode is forbidden. The strong and sharp peak at 435 cm^{-1} can be assigned to the high frequency of E_2, indicating that ZnO nanoparticles are good hexagonal oxide. The hexagonal ZnO revealed the Raman vibration at 320, 370, 405 and 575 cm^{-1}, assigned as the $E_{2H} - E_{2L}$, $A_1(TO)$, $E_1(TO)$ and $E_1(LO)$ symmetrical phonon modes, respectively. The anatase was characterized to have five Raman active modes at about 153 cm^{-1} (E_g), 203 cm^{-1} (E_g), 390 cm^{-1} (B_{1g}), 515 cm^{-1} ($A_{1g} + B_{1g}$) and 605 cm^{-1} (E_{1g}). There are five

Raman-active phonon modes (A_{1g} + E_g + $3F_{2g}$) in the cubic spinel Zn_2TiO_4, as the results summarized in Table 3.1 The Raman vibrational modes at 257, 305, 380, 470 and 722 cm^{-1} were assigned as F_{2g}, E_g, F_{2g}, F_{2g} and A_{1g} symmetrical phonon modes, respectively. $Zn_2Ti_3O_8$ has a cubic spinel structure with five Raman-active phonon modes (A_{1g} + E_g + $3F_{2g}$). The vibrations were detected at 245, 310, 470, 520 and 718 cm^{-1} and were assigned as the F_{2g}, E_g, F_{2g}, F_{2g} and A_{1g} symmetrical phonon modes, respectively. According to group theory, $ZnTiO_3$ (point group C3i) has 10 Raman active modes: $5A_g$ + $5E_g$. The Raman vibration of $ZnTiO_3$ was detected at 152, 188, 230, 262, 348, 403, 472, 486, 622 and 717 cm^{-1} and were specified as the E_g, A_g, E_g, A_g, A_g, E_g, E_g, A_g, E_g and A_g symmetrical phonon modes, respectively.

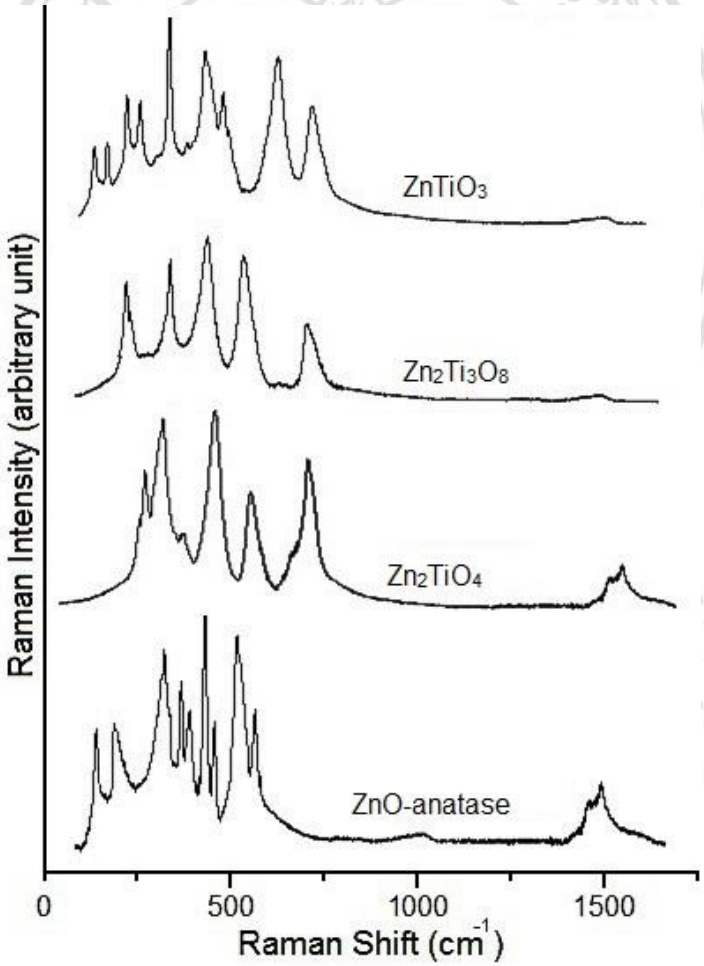

Fig. 3.8 Raman spectra of ZnO-anatase, Zn_2TiO_4, $Zn_2Ti_3O_8$ and $ZnTiO_3$.

Table 3.1 Raman active modes of this work comparing to those of the previous reports [52–55].

Samples	Assignment	Previous reports (cm^{-1})	This work (cm^{-1})
ZnO	$E_{2H} - E_{2L}$	333 [52]	320
	$A_1(TO)$	379	370
	$E_1(TO)$	409	405
	E_{2H}	437	435
	$E_1(LO)$	583	575
TiO_2	E_g	143 [53]	153
	E_g	196	203
	B_{1g}	394	390
	$A_{1g} + B_{1g}$	515	515
	E_{1g}	637	605
Zn_2TiO_4	F_{2g}	265 [54]	257
	E_g	307	305
	F_{2g}	343	380
	F_{2g}	474	470
	A_{1g}	716	722
$ZnTiO_3$	E_g	146 [55]	152
	A_g	178	188
	E_g	233	230
	A_g	267	262
	A_g	345	348
	E_g	395	403
	E_g	472	472
	A_g	485	486
	E_g	620	622
	A_g	715	717
$Zn_2Ti_3O_8$	F_{2g}	N/A	245
	E_g		310
	F_{2g}		470
	F_{2g}		520
	A_{1g}		718

3.2 **Template synthesis of Zn_2TiO_4 and $Zn_2Ti_3O_8$ nanorods by hydrothermal-calcination combined processes**

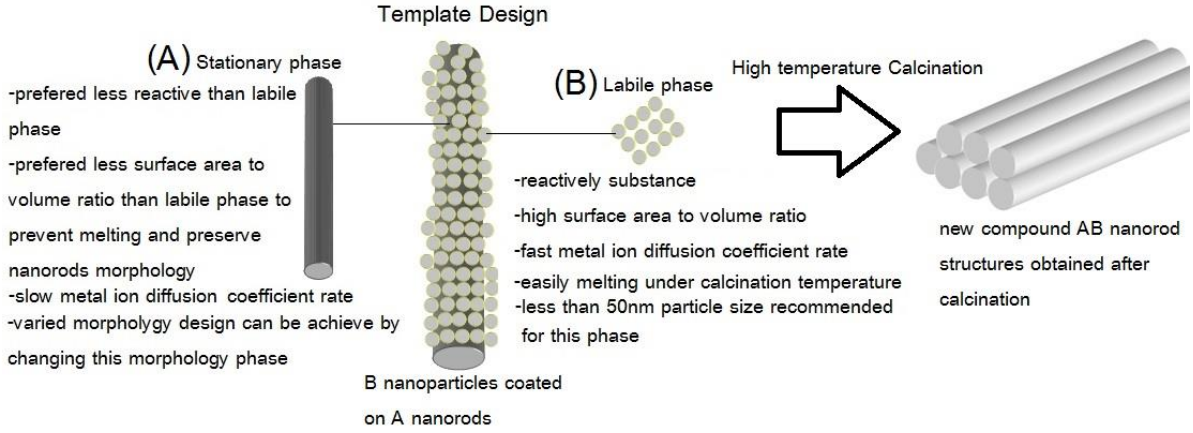

Fig. 3.9 New strategy template without using supporting materials designed for nanorod structures synthesis.

Processes for preparing highly quality of powders, better homogeneity, control morphology and smaller particle size are preferred. Moreover, ZnO nanorods were use as the template and high surface-to-volume ratio Anatase-TiO_2 nanoparticles which easily fused to form Zinc titanate under melting-point depression effect. Upon calcinations, the nanoparticles TiO_2 were fused and deposited on ZnO nanorods surface then Zinc titanate nanorods were obtained.

The ZnO-TiO_2 nanocomposites precursor autoclaved at 120 ^oC 12h by hydrothermal process shows the XRD spectra in Fig.3.10 (a) Zn:Ti The product consists of Wurtzite-ZnO and Anatase-TiO_2 was explained by the nucleation of TiO_2 which was begin with $C_4K_2O_9Ti{\cdot}2H_2O$ were dissolve in 100mL D.I. Water's pH starting drop down to 4.3, Titanium metal ions exist in aqueous solution often with the formula TiO^{2+}.

$$C_4K_2O_9Ti{\cdot}2H_2O \rightarrow 2K^+ + TiO^{2+} + 2C_2O_4^{2-} + 2H_2O \qquad (3.7)$$

When the pH was increased by the drop wise of NH_4OH, titanium hydroxide complexes precipitated.

$$TiO^{2+} + NH_4^+ + 3OH^- \rightarrow Ti(OH)_4 + NH_3 \qquad (3.8)$$

Titanium (IV) hydroxide was easily hydrolyzed to form anatase titanium dioxide and water by hydrothermal heating.

$$Ti(OH)_4 \rightarrow TiO_2 + 2H_2O \quad (3.9)$$

At the same time, ZnO nanorods were synthesized, nucleated and grew in NH_4OH alkaline solution. At the pH range of 7-9.5, some white solid was detected in the solution due to the following chemical formation.

$$Zn^{2+} + 2OH^- \rightarrow Zn(OH)_2 \quad (3.10)$$

The precipitates started to dissolve and become transparent solution again, explained by excessive NH_3 from NH_4OH by crystal-field splitting as follows.

$$Zn(OH)_2 + 4NH_3 \rightarrow [Zn(NH_3)_4]^{2+} + 2OH^- \quad (3.11)$$

During the 120 ºC and 12 h hydrothermal reaction, $[Zn(NH_3)_4]^{2+}$ was substituted by the excessive OH^- in the solution due to the evaporation of NH_3 heating.

$$[Zn(NH_3)_4]^{2+} + 4OH^- \rightarrow [Zn(OH)_4]^{2-} + 4NH_3 \quad (3.12)$$

$[Zn(OH)_4]^{2-}$ further decomposed from high pressure and temperature inside the hydrothermal bomb.

$$[Zn(OH)_4]^{2-} \rightarrow ZnO + H_2O + 2OH^- \quad (3.13)$$

Upon cooling the system down to room temperature ZnO nanorods (JCPDS No. 05-0664 Hexagonal ZnO [48]) was obtained, this can explained by the doping of La^{3+} which can produce Oxygen vacancies in ZnO structure. These vacancies will attract OH^- in the solution and lead the nuclei to rapidly form in a single direction which were explained the oxygen vacancies were generated at the top site of hexagonal ZnO structure.

In the end, the ZnO-TiO_2 nanocomposites were produced. ZnO-TiO_2 nanocomposites with different mole ratios were further calcined at 750 ºC for 5 h. XRD pattern of 2:1 atomic ratio Zn:Ti after calcination (Fig. 3.10) revealed the presence of all synthesized powder of face-centered cubic Zn_2TiO_4 structure corresponding to the JCPDS file no. 19-1483 [48]. For the 2:3 atomic ratio Zn:Ti, the diffraction peaks of 2θ were changed to 30.02°, 35.45°, 36.88º, 42.71º, 49.60º, 53.17º, 56.73º, 62.30º and 73.55°, as results shown in Fig. 1c. They are separately attributed to the (220), (311), (222), (400), (421), (422), (511), (440) and (533) planes of cubic phase $Zn_2Ti_3O_8$ crystals (JCPDS card No. 38-0500 [5]).

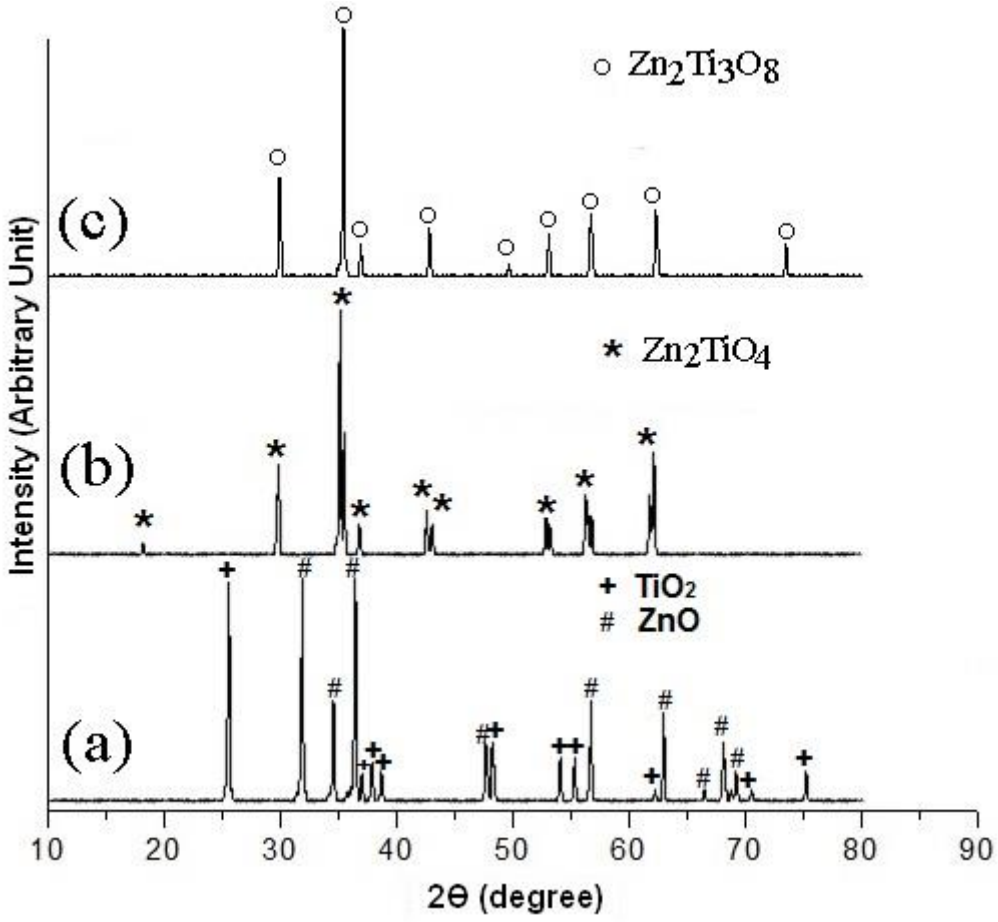

Fig. 3.10 XRD patterns of (a) ZnO-anatase obtained from hydrothermal 120 ^{o}C 12h, (b) Zn_2TiO_4 after calcinated at 750 ^{o}C for 5 h and (c) $Zn_2Ti_3O_8$ after calcinated at 750 ^{o}C for 5 h.

Basing on the chemical solution process, 0.200 mol $Zn(NO_3)_2 \cdot 6H_2O$ and 0.015 mol $La(NO_3)_3 \cdot 6H_2O$ were dissolved in 100 ml de-ionized water. NH_4OH solution was slowly added until the pH was 10. Then 0.100 mol and 0.300 mol $C_4K_2O_9Ti \cdot 2H_2O$ in 100 ml de-ionized water each was slowly mixed with the transparency solutions with keeping the pH at 10 throughout the process. These solutions were hydrothermally processed at 120 ^{o}C for 12 h. In the end, the samples were calcined at 750 ^{o}C for 5 h for further characterization.

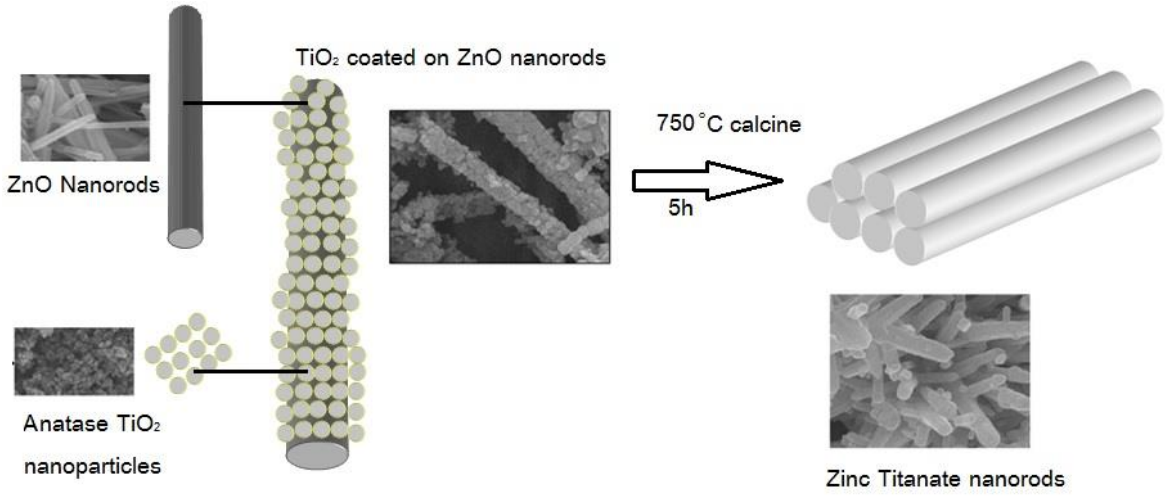

Fig. 3.11 Template method for Zinc Titanate Nanorods Struture (A) Pure ZnO Nanorods (B-C) Anatase nanoparticles start coating on ZnO nanorods (D) Anatase nanaparticles fused to ZnO nanorod to form Zinc titanate nanorods.

ZnO-TiO_2 nanocomposites from 3.2.1 with different mole ratio were further calcinations at 750 ^oC for 5 h. Zn/Ti atomic ratio of 2:1 was transformed into Zn_2TiO_4 which corresponding to JCPDS No. 19-1483 [48] and Zn/Ti atomic ratio of 2:3 was transformed into $Zn_2Ti_3O_8$ (JCPDS No. 38-0500 [48]) as in Fig. 3.10b and 3.10c due to stoichiometric effects [56] this could explain by the coating TiO_2 nanoparticles have high surface area to volume ratio than ZnO nanorods and TiO_2 which provides strong driving force under melting-point depression effect then during at higher temperature like 750 ^oC, the TiO_2 particles could be incorporated in the ZnO nanorods lattice as a solid solute at the early stages because if the faster diffusion rate of Ti^{4+} than that of Zn^{2+} [56] (Fig. 3.11) and this also explained why all zinc titanates still remain in nanorods morphology form. The XRD patterns also confirmed to indicated that $Zn_2Ti_3O_8$ was synthesized is the characteristic peak at the about 75 2Θ (degree). In the end, the ZnO-TiO_2 nanocomposites were produced. ZnO-TiO_2 nanocomposites with different mole ratios were further calcined at 750 ^oC for 5 h. XRD pattern of 2:1 atomic

ratio Zn:Ti after calcination (Fig. 3.10b) revealed the presence of all synthesized powder of face-centered cubic Zn_2TiO_4 structure corresponding to the JCPDS file no. 19-1483 [48]. For the 2:3 atomic ratio Zn:Ti, the diffraction peaks of 2θ were changed to 30.02°, 35.45°, 36.88°, 42.71°, 49.60°, 53.17°, 56.73°, 62.30° and 73.55°, as results shown in Fig. 3.10c. They are separately attributed to the (220), (311), (222), (400), (421), (422), (511), (440) and (533) planes of cubic phase $Zn_2Ti_3O_8$ crystals (JCPDS card No. 38-0500 [48]).

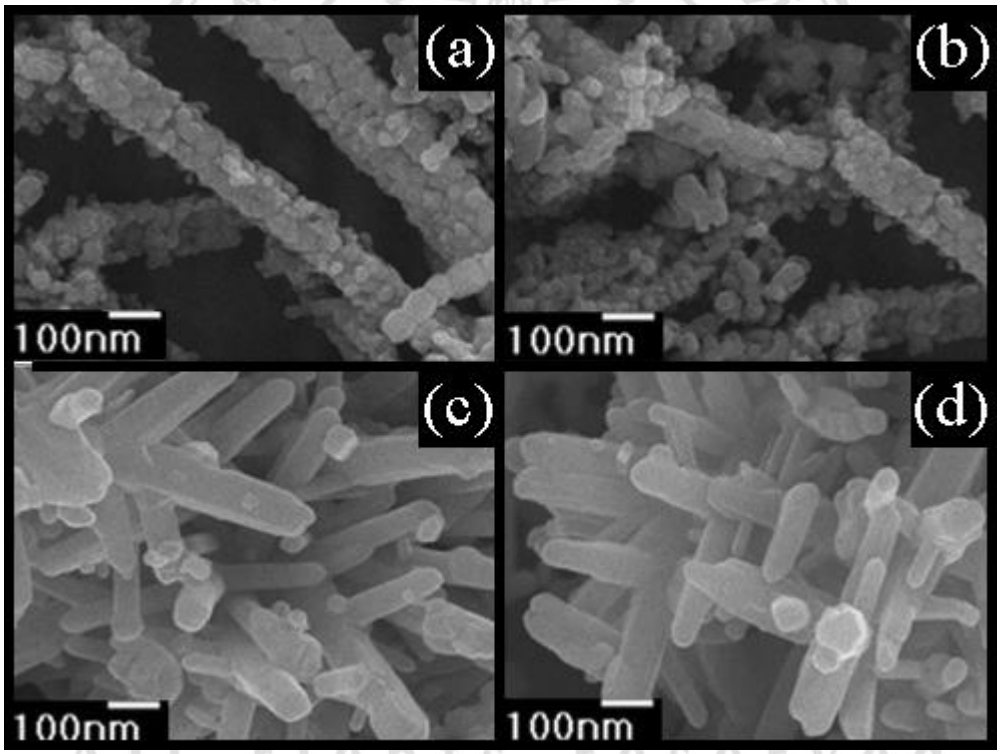

Fig. 3.12 SEM images of (a) ZnO-Anatase TiO_2 2:1, (b) ZnO-Anatase TiO_2 2:3 and (c) Zn_2TiO_4 (d) $Zn_2Ti_3O_8$.

Related to Fig. 3.12 the morphology of ZnO-anatase was nanoparticles coated on ZnO nanorod with varied size measured by particle size ratio and Surface area by BET method. As before calcinations, the precursor ZnO-Anatase TiO_2 nanocomposite in Fig.

3.12a has Surface area 112.16 m^2/g which are good enough refer to [49] to provide melting-point depression effect. After calcinations, Zn_2TiO_4 nanoparticles were obtain through agglomeration of ZnO-Anatase TiO_2 nanocomposite (2:1) at 750 ^oC for 5 h. The surface area has been decreased to 15.09 m^2/g due to the agglomerated particles were larger than the original. In solid-state reactions the reactants are initially in contact and combine chemically to form the reaction product. The kinetics of the initial stage of such a reaction depends on the parameters of the interface (e.g., the crystallography of the contacting surface, surface area). The mechanism for such reactions was proposed by Wagner (Fig. 3.13) to be the counter-diffusion of cations in ionic systems. It has been found that this mechanism does occur in the layer of ZnO due to the temperatures and the diffusion coefficient of Ti^{4+} and Zn^{2+}. Manik et al. [56] reported that Ti^{4+} has faster diffusion rate than Zn^{2+} so the TiO_2 nanoparticles will fused and incorporated to the ZnO nanorods lattice first. This is the reasons why the morphology of Zn_2TiO_4 and $Zn_2Ti_3O_8$ still remains nanorods. $Zn_2Ti_3O_8$ nanoparticles were synthesized from ZnO-Anatase TiO_2 nanocomposite(2:3) at 750 ^oC for 5 h, the surface area has decreased to 10.45 m^2/g. Their morphologies before and after calcination were investigated by scanning electron microscopy (SEM), as the results shown in Fig. 3.12. Before calcination, ZnO-TiO_2 nanocomposites show nanoparticles TiO_2 coated on ZnO nanorods (Fig. 3.12a and 3.12b). Upon calcination at high temperature, Zn_2TiO_4 and $Zn_2Ti_3O_8$ (Fig. 3.12c and 3.12d) show nanorods in shape. The formation of zinc titanate was proposed by the Wagner's cation counter diffusion reaction mechanism model [57]. It has been found that Ti^{4+} and Zn^{2+} diffuse across the ZnO layer during high temperature calcination. Manik et al. [56] reported that Ti^{4+} diffuse faster than Zn^{2+}. Therefore, the TiO_2 nanoparticles are able to be fused and incorporated to the ZnO nanorods first. Thus Zn_2TiO_4 and $Zn_2Ti_3O_8$ still remain as nanorods.

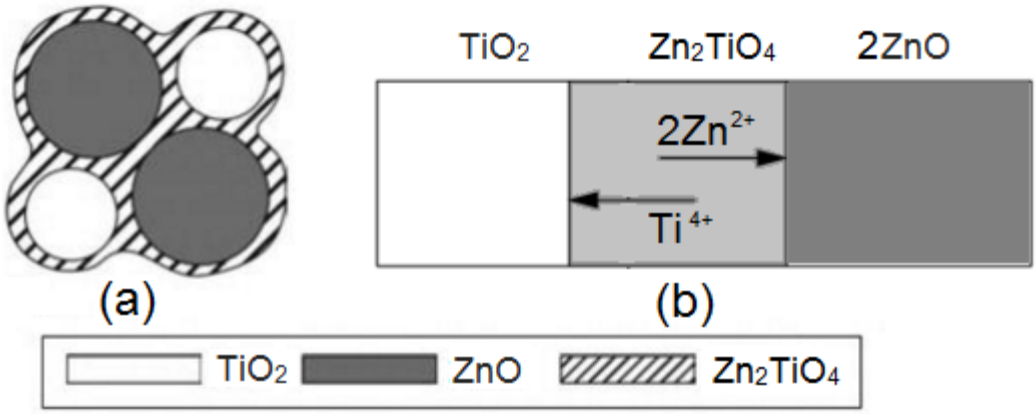

Fig. 3.13 Interface solid-state reaction for the growth of Zinc Titanate. (a) Conventional particles reaction where ZnO-TiO_2 are mixed thoroughly and calcinated at 750 ^oC. (b) Proposed schematic diffusion Ion of Zn^{2+} and Ti^{4+} by using Wagner's cation counterdiffusion reaction mechanism model. [57]

Zinc titanate form at the contact face in which the material transport methods involve volume and surface diffusion, grain boundary diffusion, and evaporation and deposition. (b) Wagner counter diffusion [57] schematics applied for ZnO-TiO_2 diffusion mechanisms during the zinc titanate-forming solid-state reactions.

Zinc orthotitanate nanorods and zinc polytitanate nanorods were synthesized via hydrothermal-calcination combined processes by the reaction of ZnO nanorods as a template coated with anatase TiO_2 nanoparticles. According to the experimental results, the zinc titanate nanorods were developed via high surface area to volume ratio TiO_2 nanoparticles incorporated into lattice of ZnO nanorods template, remained as nanorods. The precursors ZnO-TiO_2 nanocomposites were successfully synthesized by a hydrothermal method. Subsequently, they were transformed into Zn_2TiO_4 nanoparticles by calcining of ZnO-TiO_2 with 2:1 mole ratio at 750 ^oC for 5 h. The $Zn_2Ti_3O_8$ sample was able to be synthesized by calcination of ZnO-TiO_2 with 2:3 mole ratio at 750 ^oC for 5 h.

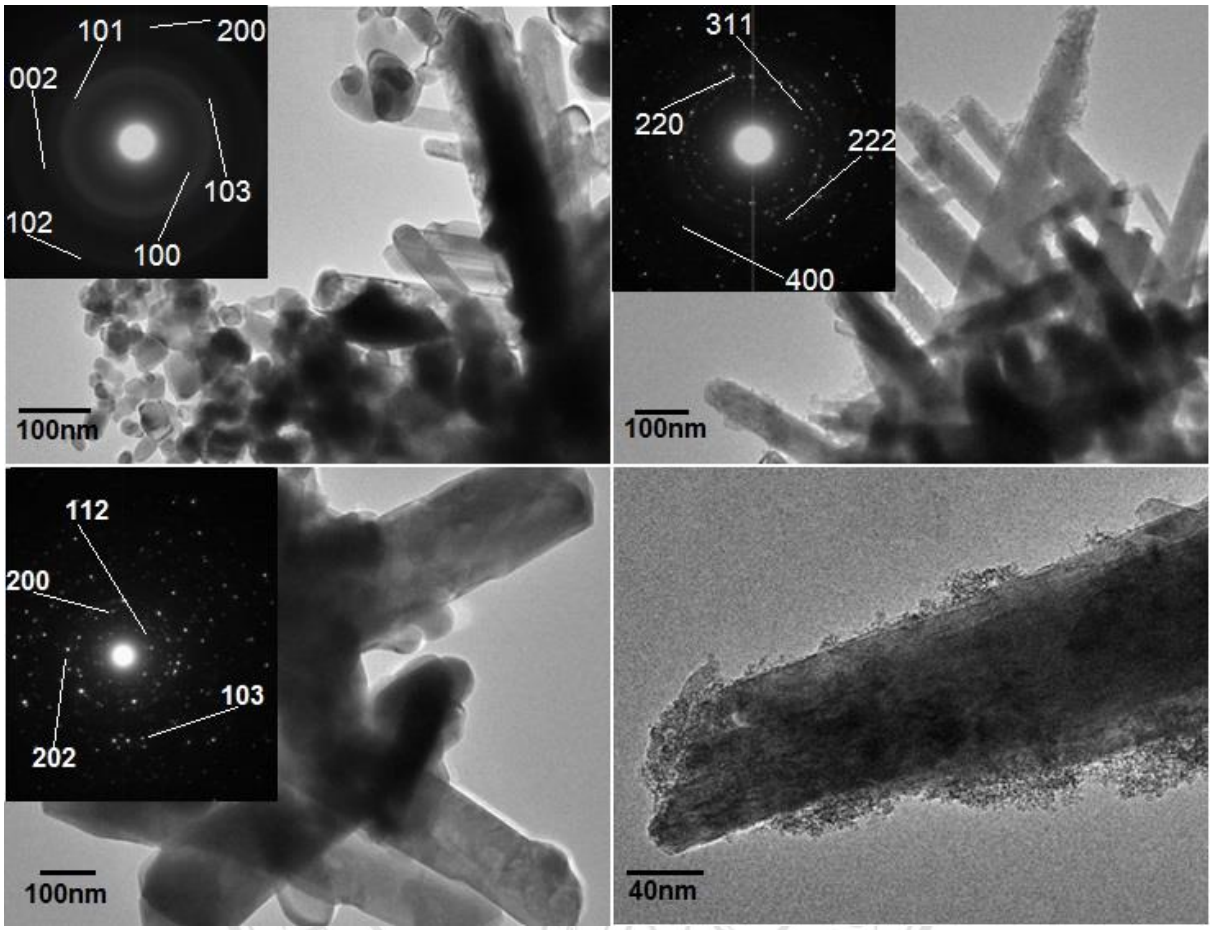

Fig. 3.14 TEM and SAED images of (a) ZnO-Anatase TiO_2, (b-c) Zn_2TiO_4 and (d) $Zn_2Ti_3O_8$

To further understand the nanostructure of ZnO-Anatase TiO_2 (before calcinations) in Fig. 3.14a illustrates the TEM bright field image are very small diameter nanoparticle anatase morphology (20-40nm) and ZnO nanorods which corresponding to selected are diffraction image in Fig. 3.14a. After calcination, the melting temperature (T_m) of nanoparticle material, surface effects on T_m can be regarded to nanoparticles which the surface area-to- volume ratio is large and the surface curvature is high, T_m is size dependent are the main factors to synthesis under lower temperature calcination. This behavior has been explained by thermodynamics theory and shown by some experimental [58]. In Fig. 3.14b shows Zn_2TiO_4 with varied size of nanorods in the diameter range of 50-100 nm and the corresponding selected area diffraction (SAD) ring-pattern verify that Zn_2TiO_4 is in the structure as shown by Fig. 3.14b compose of the lattice fringes of 222, 220, 311 and 400, which is the same as that of XRD

observation. Manik[57] reported that TiO_2 was like the mobile phase that the TiO_2 islands could be incorporated in the ZnO lattice solute at the first stage because of the faster diffusion rate of Ti^{4+} than that of Zn^{2+} then Zn_2TiO_4 spinel nanocrystallites formed through lattice rearrangement. Unlike the reaction of ZnO-Al_2O_3 nanowires [59] no voids or tubular structures appeared at the ZnO/Zn_2TiO_4 surface indicating that the in-diffusion of Ti^{4+} is dominating for the TiO_2/ZnO thermal couple as expected. Yang et al [60] also explained the mechanism through careful TEM investigation that the initial anatase-TiO_2 particles on the surface of ZnO nanorods transform into anatase TiO_2 islands, which are isolated from each other as a result of crystallization-induced volume shrinkage then incorporated into the ZnO lattice as segregation and reacts into individual spinel crystallites through lattice rearrangement. These spinel bricks are attached to the surface of the unconsumed ZnO stem. Finally, the unreacted ZnO is evaporated through the gaps of the bricks [59] then reacted with another anatase islands until complete due to stoichiometry effects. All the bricks will then assemble into solid nanorods via an oriented attachment and coalescence (Ostwald ripening). In Fig 3.14c HRTEM of Zn_2TiO_4 show [0001] plane growth direction which was the same when refer to oxygen vancancies in ZnO nanorods rapid growth direction [61]. $Zn_2Ti_3O_8$ in Fig. 3.14d shows nanorods morphology within the diameter size of 50-100 nm and corresponding selected area diffraction in Fig. 3.14c illustrates ring-pattern of 103, 200, 112 and 202 Lattice fringe.

ZnO:TiO_2 (2:3) in fig. 3.15a was detected by EDX spectrometer equipped in Scanning electron microscope in Fig. 3.12. The atomic percentage showed atomic ratio of Zn:Ti was 1:1.5 which corresponding to ZnO:TiO_2 (2:3). After calcinations ZnO:TiO_2 (2:3), $Zn_2Ti_3O_8$ was obtained the atomic percentage showed ratio of Zn:Ti was still 2:3 same as the precursor but some oxygen percent were loss due to dehydration from heat during calcinations reaction. Base upon doping theory [61], the dopant should not appear in XRD as in Fig. 3.10 that confirmed there is none of trace La was detected but the trace of La should be detected by EDX spectra as in Fig. 3.15 to confirm that La elements were not form of Lanthanum compounds but La^{3+} instead which confirmed La was incorporated in the matrix structure donor compound. We also found that using La-doped ZnO and La-doped TiO_2 as the precursor will make Zinc titanates was doped by La too as in the Fig. 3.15b.

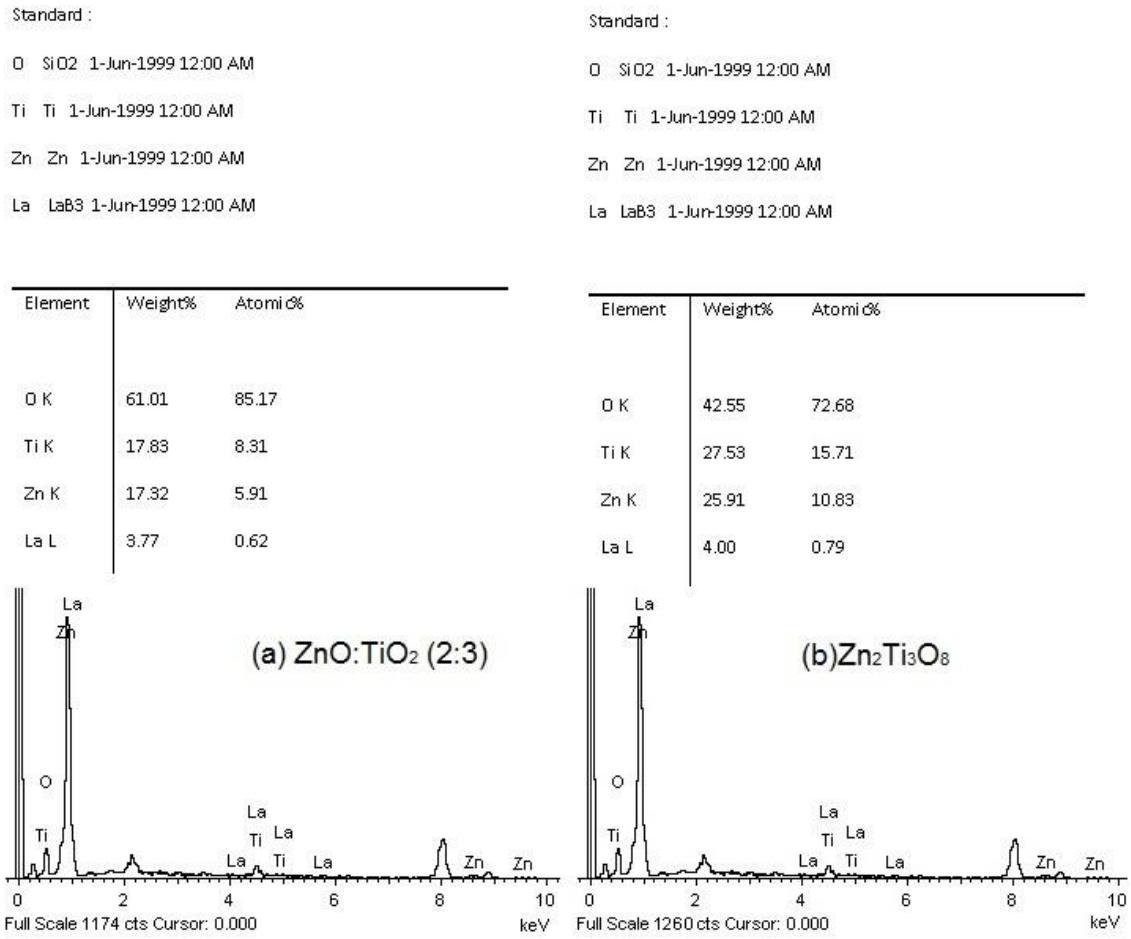

Fig. 3.15 EDX spectra of (a) ZnO-TiO_2 nanocomposites (2:3) and (b) $Zn_2Ti_3O_8$